

**Enigmatic tsunami waves amplified by repetitive source events in the southwest of
Torishima Island, Japan**

**Osamu Sandanbata^{1†}, Kenji Satake¹, Shunsuke Takemura¹, Shingo Watada¹, and Takuto
Maeda²**

¹Earthquake Research Institute, The University of Tokyo, Tokyo, Japan.

²Graduate School of Science and Technology, Hirosaki University, Aomori, Japan.

Corresponding author: Osamu Sandanbata (osm3@eri.u-tokyo.ac.jp)

Key Points

- On 9 October 2023 (JST), enigmatic tsunamis up to ~60 cm were recorded along broad Japanese coasts without large earthquakes.
- Analysis of stacked bottom-pressure data shows >10 repetitive events for ~1.5 hr intermittently produced tsunamis with T-phase excitation.
- Larger events in later sequence occurred with intervals similar to the wave period, amplifying the tsunami waves in later phase.

Abstract

On 9 October 2023 (JST), mysterious tsunamis with a maximum wave height of 60 cm were observed in Izu Islands and southwestern Japan, although only seismic events of body-wave magnitudes m_b 4–5 have been documented in the southwest of Torishima Island. To investigate the source process, we analyze tsunami waveforms recorded by an array network of ocean-bottom pressure gauges. A stacked waveform of 16 records suggests recurrent arrivals of multiple wave trains. Deconvolution of the stacked waveform by a tsunami waveform from the first event revealed over 10 source events that intermittently generated tsunamis for ~ 1.5 hours. The temporal history of this sequence corresponds to the origin times of T-phases estimated by an ocean-bottom seismometer, and the m_b 4–5 seismic swarm, implying a common origin. Larger events later in the sequence occurred at intervals comparable to the tsunami wave period, causing amplification of later phases of the tsunami waves.

Plain Language Summary

On 9 October 2023 (JST), mysterious tsunamis hit Izu Islands and southwestern Japan, reaching up to 60 cm in height, although only small-to-moderate seismic events were reported in the region. To resolve how the mysterious tsunami waves were generated, we analyze the waves recorded by a tsunami observation network off the southwestern coast of Japan. We find that the tsunami waves were intermittently produced by repetitive source events for approximately 1.5 hours, and the wave amplification happened because the event interval time matched the wave period. These abnormal submarine events excited significant acoustic oceanic waves, as well as large tsunamis, which would provide valuable information to further study what took place in the ocean.

41

42 **1 Introduction**

43 On 9 October 2023 (JST, +09UTC), enigmatic tsunamis were observed along coasts in
44 broad region from south to west of Japan. The tsunami heights, measured from zero to crest,
45 were 30–60 cm in Izu Islands (Yaene, Tsubota, and Kozushima) and the Kanto region (Mera),
46 and 30–40 cm tsunamis were recorded even in distant stations (Tosa-shimizu and Nakanoshima)
47 (Japan Meteorological Agency, 2023) (Figure 1a). Because no significant earthquake was
48 observed and no offshore tsunami observation system is deployed off Izu-Bonin Islands, the
49 tsunami forecasting system did not work well; it was only after the tsunami was clearly recorded
50 by a tsunami-meter at Yaene on Hachijojima Island that the tsunami advisory was issued by
51 Japan Meteorological Agency (JMA).

52 From 3:58 to 6:21 (JST) on the day, 13 small-to-intermediate seismic events of body-
53 wave magnitudes m_b 4.3–5.4 in the oceanic region approximately 80 km southwest of Torishima
54 Island were reported in the earthquake catalog of U. S. Geological Survey (USGS; Figure 1c);
55 here, these seismic events are labelled as *Se01–13* (Table S1). The amplitudes of the observed
56 tsunamis were by far larger than those expected from the seismic magnitudes; the tsunami
57 magnitude based on the maximum amplitude information reported by JMA is estimated as M_t 8.0
58 (Abe, 1981). This fact suggests the atypical source mechanism of the tsunamis. For such
59 tsunamis without large earthquakes, various types of source mechanism have been proposed: for
60 example, slow-ruptured tsunami earthquakes along subduction zones (e.g., the 1896 Sanriku
61 earthquake, the 1946 Aleutian earthquake) (Kanamori, 1972; Tanioka & Satake, 1996), oceanic
62 volcanic processes (e.g., the 2018 Anak Krakatau eruption, the 2022 Hunga Tonga–Hunga
63 Ha‘apai eruption) (Kubota et al., 2022; Mulia et al., 2020; Paris, 2015), or submarine/coastal

landslides or mass failures (e.g., the 1998 Papua New Guinea tsunami) (Synolakis et al., 2002; Tappin et al., 1999).

In this study, we investigate the source process of the enigmatic tsunami waves using tsunami waveform data recorded by an array network of ocean-bottom-pressure (OBP) gauges off the southwestern coast of Japan. We first apply a waveform stacking technique to the multiple tsunami waveforms, and then estimate the temporal history of the tsunami generation based on analysis of the stacked data. Consequently, we propose their peculiar tsunami origin by repetitive source events that took place intermittently for ~ 1.5 hours.

2 Data

The tsunami waves were recorded by the dense OBP gauges of Dense Oceanfloor Network system for Earthquakes and Tsunamis (DONET) off the southwestern coast of Japan (Figure 1b) (National Research Institute for Earth Science and Disaster Resilience, 2019). In Figure 2a, we show the OBP data after removing the tidal component, demonstrating repetitive strong high-frequency signals with dominant frequencies of higher than 1 Hz approximately from 4:00 to 6:30 (see Figure S1). These high-frequency signals are confirmed to be T-phases, seismic waves converted from oceanic acoustic waves (Okal, 2008), based on their arrival times explained by a typical T-phase speed of 1.5 km/s from the origin times and locations of the seismic events. Following the T-phase signals, tsunami waves with longer periods were recorded, as shown evidently in the band-pass (0.00125–0.02 Hz/50–800 s) filtered records (Figure 2b). Smaller oscillations start around 5:40, leading to the largest amplitudes of ~ 20 mm after $\sim 7:00$. Thus, the tsunami oscillations continued for hours with late arrivals of large amplitude waves.

To capture the features, a tsunami waveform stacking technique is applied to 16 OBP records of DONET1, listed in Table S2. By assuming a point source at the epicenter location (140.026°E, 29.787°N) of the m_b 5.4 seismic event (Se12), the largest event among the swarm, the tsunami travel times to the OBP gauges are computed by a shallow-water-wave tsunami model of the Geoware TTT Software (Figure S2). The band-pass filtered waveform at each OBP is shifted in such a way that the arrival times are aligned with that at the earliest-arrival station (KMC21). We then stack the time-shifted waveforms and take the amplitude average and standard deviation.

As shown in Figures 3a and 3b, all the OBP waveforms used here show similar shapes; thereby, the waveform stacking yields clear tsunami waveforms only with small standard deviations. The tsunami waves initiate at ~120 min (~5:30) and reach the maximum amplitude at ~220 min (~7:10).

For further investigation, we apply the wavelet analysis to the stacked waveform (Figure 3c). The obtained scalogram shows that the tsunami signals are composed of multiple bands of dispersive amplitude peaks with early arrival of lower-frequency amplitude followed by higher-frequency amplitude (red arrows and a curly bracket in Figure 3c). This character with multiple bands is quite different from a tsunami event originating from a single volcanic earthquake at Sumisu Caldera, which shows only a single band (Figures S3; see the caption for details). Therefore, we speculate that multiple tsunami wave trains, each with a strongly dispersive character, recurrently arrived at the OBP gauges.

3 Estimation of source time function

We investigate the temporal history of the tsunami generation process by using the iterative deconvolution method (Kikuchi & Kanamori, 1982), widely applied for earthquake source studies.

We hypothesize that multiple impulsive source events took place at the same location but at different timings, and that each single event produced tsunami waveforms with the same shapes and different amplitudes. Under this hypothesis, the stacked OBP tsunami waveform is the convolution of the temporal history of multiple impulsive events, or the *tsunami source time function* (STF), and the tsunami waveform produced by a single event, or the *Green's function*. Denoting the stacked tsunami waveform as $d(t)$ and the Green's function as $w(t)$, the convolution can be expressed, as follows:

$$d(t) = \sum_i m_i w(t - t_i), \quad (1)$$

where m_i and t_i represent the source amplitude and the timing of the i -th source event (note that i represents the iteration time, not the order in time, as explained below).

The Green's function is extracted from the stacked tsunami waveform data. We first confirm that the theoretical arrival times of the tsunamis caused by the two early earthquakes, Se02 and Se03 (Table S1), agree well with the timings when the tsunami signal initiates (~5:40) and when the amplitude increases (~6:00), respectively (arrows in Figure 4a). We assume that the signal between the two tsunami arrival times represent the tsunami waveform due to Se02, and construct the Green's function with an initial zero-amplitude data for the length of the theoretical tsunami travel time, followed by the stacked waveform in the time window (with tapering on the 5% edges) (green line in Figure 4a). m_i in Equation (1) now represents the

relative source amplitude of the i -th source event to that of Se02, and we impose $m_i \geq 0$ under our hypothesis of multiple similar events.

Using the Green's function, we deconvolve the stacked tsunami waveform (Figure 4a) to estimate the tsunami STF, following Kikuchi and Kanamori (1982). Denoting the stacked tsunami waveform as $x(t)$, we first take a single event and determine m_1 and t_1 by minimizing the error defined as:

$$\Delta_1 = \int_0^T [x(t) - m_1 w(t - t_1)]^2 dt, \quad (2)$$

where T is the length of the stacked waveform, and obtain the residual waveform:

$$x^{(1)}(t) = x(t) - m_1 w(t - t_1). \quad (3)$$

In the next iteration, we determine m_2 and t_2 by minimizing the error Δ_2 for the residual waveform $x^{(1)}(t)$, and obtain the residual waveform:

$$x^{(2)}(t) = x^{(1)}(t) - m_2 w(t - t_2). \quad (4)$$

We iteratively repeat the procedure above until the approximation error changes by less than 2% by an iteration $((\Delta_{i-1} - \Delta_i)/\Delta_{i-1} < 0.02)$. The approximation accuracy is quantified by the normalized approximation error by

$$\Delta_i/\Delta_0 = \int_0^T [x^i(t)]^2 dt / \int_0^T [x(t)]^2 dt. \quad (5)$$

Thus, we determine the relative source amplitudes of m_i at the timings of t_i ($i = 1, \dots, N$).

We find that, in the iterative deconvolution process, the source amplitudes determined in earlier iterations tend to be larger, because the original observed waveform is fit mainly by earlier-determined events, and later events are fit to the residual waveforms (Kikuchi & Kanamori, 1982). As seen in the iterative deconvolution results (Figure S4), a source event at

6:17, determined in the first iteration, has a very large source amplitude. To examine how reliable the results are, we re-determine the source amplitudes by an additional least-squares method. While fixing the source event times t_i , we re-estimate the source amplitude m'_i by minimizing the following error by the non-negative least-squares method:

$$x(t) - \sum_{i=1}^N m'_i w(t - t_i). \quad (6)$$

Thus, we obtain the tsunami STF, represented by the relative source amplitude m'_i at the source times of t_i . The tsunami waveform is modeled with Equation (1), where m_i is replaced by m'_i . The additional least-squares method improves the amplitude balance of several source events close in time, determines the amplitude of an event as zero, which we remove from the event list; then, the normalized approximation error is reduced significantly from 0.174 to 0.118 (compare Figure S4 with Figure 4).

4 Results

We obtain the tsunami STF composed of 23 single-source events that span from 4:54 to 7:02, labeled as *Ts01–23* (Figure 4 and Table S3). The fit between the stacked waveform and the convolved waveform is remarkably good (Figure 4b). This suggests that repetitive tsunami source events took place with a similar mechanism at similar locations, intermittently producing similar tsunami waveforms.

Major source events are estimated from 4:54 (Ts01) to 6:34 (Ts18) for over 1.5 hours (Figure 4c). Some of these events are close to each other with a time difference of only $< \sim 100$ s (Ts06–07, and Ts09–10). These may be separately deconvolved from a single event due to unmodeled later phases of prior events (e.g., coastal reflected waves), not included in the Green's function. Given the limitation, we exclude Ts06 and Ts10, a smaller event among each pair, from

major events. Later events, Ts19–23, may be also artifacts arising for the same reason. Then, the sequence of the major events gradually increases the amplitude from 1.0 to 6.5 and reduces the interval time approximately from 1,200 s to 250 s.

Most of the later major events with larger amplitudes (e.g., Ts11–15) occur with interval of 200–300 s (Figure 4c, and Table S3), which are comparable to the dominant period of the observed tsunami waveforms (Figure 3c). Figure 5a shows tsunami waveforms from Ts11–15, each of which has a non-negligible amplitude of ~ 10 mm, less than half of the amplitude of the stacked largest waves between 7:00 and 7:20. Yet, their waveform phases match with each other, and thereby the superposition of the tsunami waveforms doubles the wave amplitude and reproduces the largest waves (Figure 5b). Therefore, the late arrivals of large tsunami waves can be attributed to the later large events with interval times similar to the characteristic period of the tsunami waves.

The major source events in the tsunami STF correlate well with the swarm of seismic events. In Figure 4d, we compare the tsunami STF with the sequence of seismic events Se01–13, reported in the USGS catalog (Table S1). Each of the seismic events of Se02–13, excluding Se01, nearly coincides with one of the major tsunami source events, Ts01–15. The overall trend in event size is also similar to that of the tsunami STF.

As shown in Figure 2a, strong T-phase signals were repetitively recorded. We investigate their origins by analyzing the up-down component of a broadband seismometer at KMB06 (Figure 1b); we first apply the band-pass (1–6 Hz) filter, convert the waveform into envelope by the Hilbert transform and the moving average with a 5-s window, and identify T-phase signals with a maximum amplitude larger than an empirical threshold of 2.0×10^3 nm/s. The origin times of the T-phase signals are determined by shifting the maximum amplitude time backward by the

travel time from the Se12 location to KMB06 (5.48 min). As results, we detect 14 T-phase events, labeled as *Tp01–14*, as listed in Table S4. The temporal history of the T-phase events, except for *Tp01*, agrees with the tsunami STF, as well as the seismic event swarm (Figure 4d), in terms of the origin times and the overall trend in size.

5 Discussion & Conclusions

Table S5 summarizes 14 source events (labeled as *EV01–14*), which have similar origin times based on data of tsunami waves, seismic waves, and T-phases. *EV01* at ~4:00 and *EV11* at ~6:09 are missing in the tsunami STF and in the USGS catalog, respectively, whereas all the other events are commonly detected as tsunami and seismic wave, and T-phase sources. Note that the envelope shape of the T-phase signal from *EV01*, or *Tp01*, indicates its longer source duration than those of the others (Figure 4d and Table S4); this may explain why *EV01* did not generate noticeable tsunami waves, since a long-duration tsunami generation process with a small source area cannot displace the water height efficiently (Saito & Furumura, 2009).

We have revealed that the repetitive events excited strong acoustic (*P*) waves that are converted to T-phases and generated large tsunami waves, but radiated only minor seismic waves equivalent to m_b 4–5. Although the mechanism of the repetitive events remains to be solved, the coincidental excitation of strong T-phases and large tsunamis suggests a very shallow source depth in the crust or just on the seafloor. T-phase data may constrain the water depth where the events took place, because T-phases are more effectively excited in a water depth of ~1,000 m, a range of the so-called SOFAR channel (Okal, 2008). On the other hand, the tsunamigenesis requires a large volume of displaced seawater by such as seafloor deformation or mass movement on the seafloor. Several possible candidates that satisfy both conditions remain. Volcanic processes in the ocean, ranging from eruptions (Purkis et al., 2023; Yamasato et al.,

1993), flank failures (Grilli et al., 2019), intra-caldera faulting (Sandanbata et al., 2023), and caldera collapse (Maeno et al., 2006) may explain these characters. Repetitive T-phase events following a non-double-couple earthquake (M_w 5.7) in 1996 near Sumisu Caldera (Figure 1c), which caused a large tsunami, were attributed to submarine volcanic phenomena (Sugioka et al., 2000). Submarine landslides or mass failures can be also possible, as T-phases were recorded around the timing of the 1998 Papua New Guinea tsunami (Okal, 2003). Faulting events cannot be excluded from candidates, but in this case, the source depth must be very shallow in the crust, given the low seismic excitation (Fukao et al., 2018). A compilation of different datasets of tsunamis, seismic waves, and T-phases would be the key to determine the mechanism. More direct information may be obtained by ship-borne surveys of the bathymetry change in the source region.

The character of the repetitive events is informative to know how the series of phenomena proceeded. As seen in Figures 5c and 5d, the source event number increases exponentially with time; in other words, the inter-event interval of the events exponentially decreases. Geological phenomena with similar characteristics of decreasing inter-event interval were previously reported as precursors for landslide events (Yamada et al., 2016), collapse events of volcanic calderas (Michon et al., 2009), and for fault slip in a critical state in tectonic environment (Igarashi, 2000).

The 9 October 2023 tsunami followed a previous seismic swarm mainly from 2 to 6 October, including two $M_w > 6$ earthquakes in the source region (Figure 1c). The relationship between the tsunami event and the preceding swarm is unclear, but we note that some earthquakes on 5 October radiated much stronger seismic waves than the 9 October sequence, although signals in the frequency range of 1–4.99 Hz, where T-phase are dominant, are larger for

the latter (compare Figures S1 and S5), indicating a big difference in their source mechanisms or source depths. One possible hypothesis for the link is that the seismic swarm was related to the movement of magma in the crust, leading to another phase of volcanic process, such as underwater eruptions, volcanic deformation, or flank collapses. Another is that ground shaking due to the preceding swarm destabilized parts of sloped bathymetry in this region, leading to submarine mass failures a few days later.

The enigmatic tsunami event on 9 October 2023 sheds light on the difficulty in forecasting the types of tsunamis not accompanying any significant earthquake in the Izu-Bonin region, where no offshore tsunami observation system is deployed. The coincidence of strong T-phases with tsunami generation may help us to estimate the tsunami potential in advance, as has been long suggested (Ewing et al., 1950; Matsumoto et al., 2016). However, the Izu-Bonin region hosts a number of volcano islands, submarine volcanoes, and active back-arc rift systems (Kodaira et al., 2007), suggesting various types of potential tsunami hazards. Previously, another series of peculiar tsunamis have recurrently taken place, almost every 10 years, due to M_w 5.4–5.8 volcanic earthquakes at Sumisu Caldera, ~100 km north of Torishima Island (Figure 1c) (Kanamori et al., 1993; Satake & Kanamori, 1991); a submarine trapdoor faulting in the caldera was recently proposed for the series (Sandanbata et al., 2022). In another case, an M_w 6.4 normal faulting earthquake on 24 October 2006 in a region between Sofugan and Nichiyo Seamount (Figure 1c) also caused about 10-cm tsunamis (Japan Meteorological Agency, 2023). In this context, there is an urgent need to improve preparedness for potential tsunami occurrences in the oceanic region.

Acknowledgments

We thank Tatsuhiko Saito for helping to develop the waveform stacking method. This work is funded by the Sasakawa Scientific Research Grant from The Japan Science Society (Grant number 2023–2031).

Data availability

DONET data is available from NIED (National Research Institute for Earth Science and Disaster Resilience, 2019) (<https://www.seafloor.bosai.go.jp/>). We use bathymetric data of JTOPO30, which are available from the Japan Hydrographic Association (<http://www.mirc.jha.jp/products/finished/JTOPO30/>). Earthquake information is available from U. S. Geological Survey (USGS: <https://earthquake.usgs.gov/earthquakes/search/>, accessed on 19 October 2023).

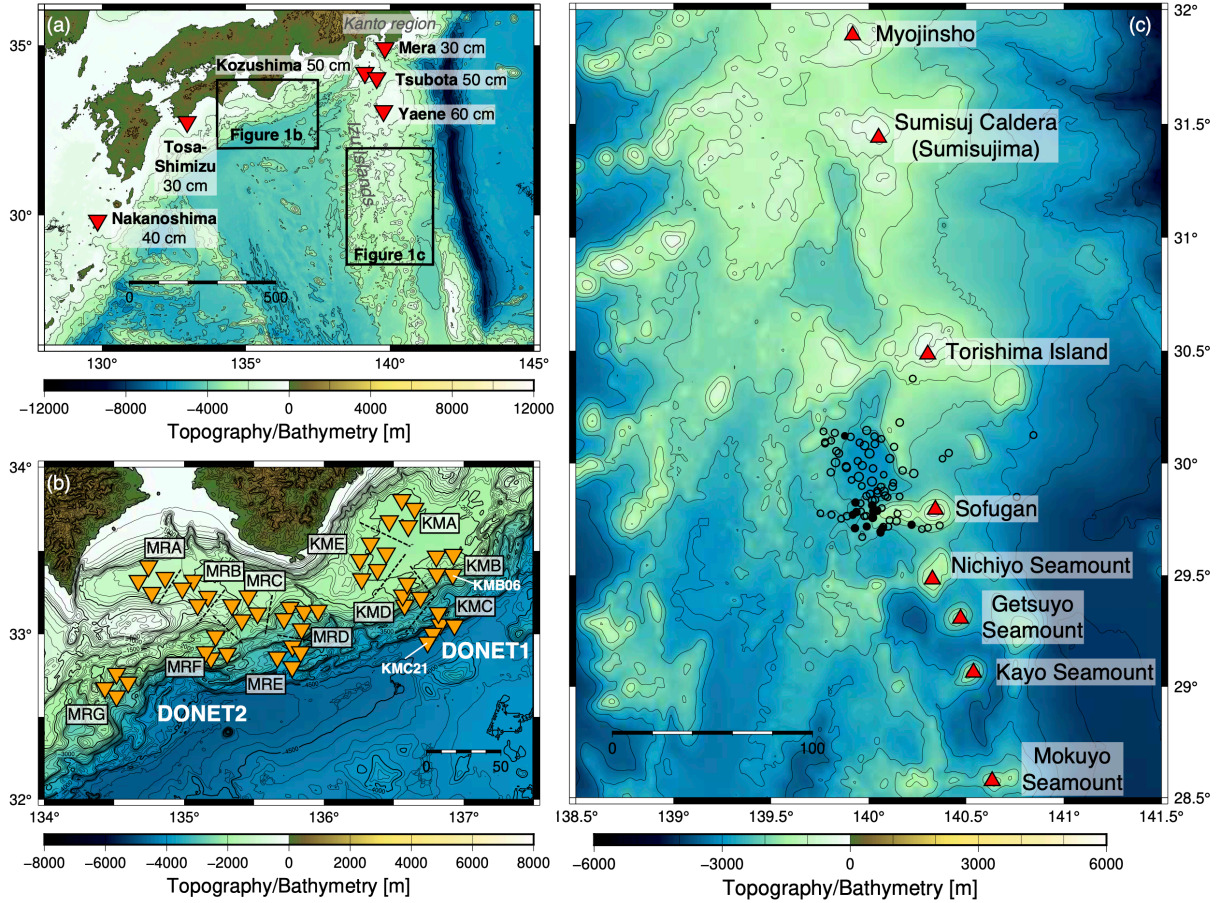


Figure 1. Maps of the study area. (a) Philippine Sea off southwestern Japan region. Red inverted triangles represent locations of tide gauges with the maximum tsunami heights reported by JMA. (b) Orange inverted triangles represent the DONET stations. (c) The region near Torishima Island. Black open and closed circles represent the locations of seismic events at depths of <20 km from 2 to 8 October 2023 (JST), and on 9 October 2023, respectively, reported in the USGS earthquake catalog. Red triangles represent active volcanoes documented in (Hydrographic and Oceanographic Department, Japan Coast Guard, 2006).

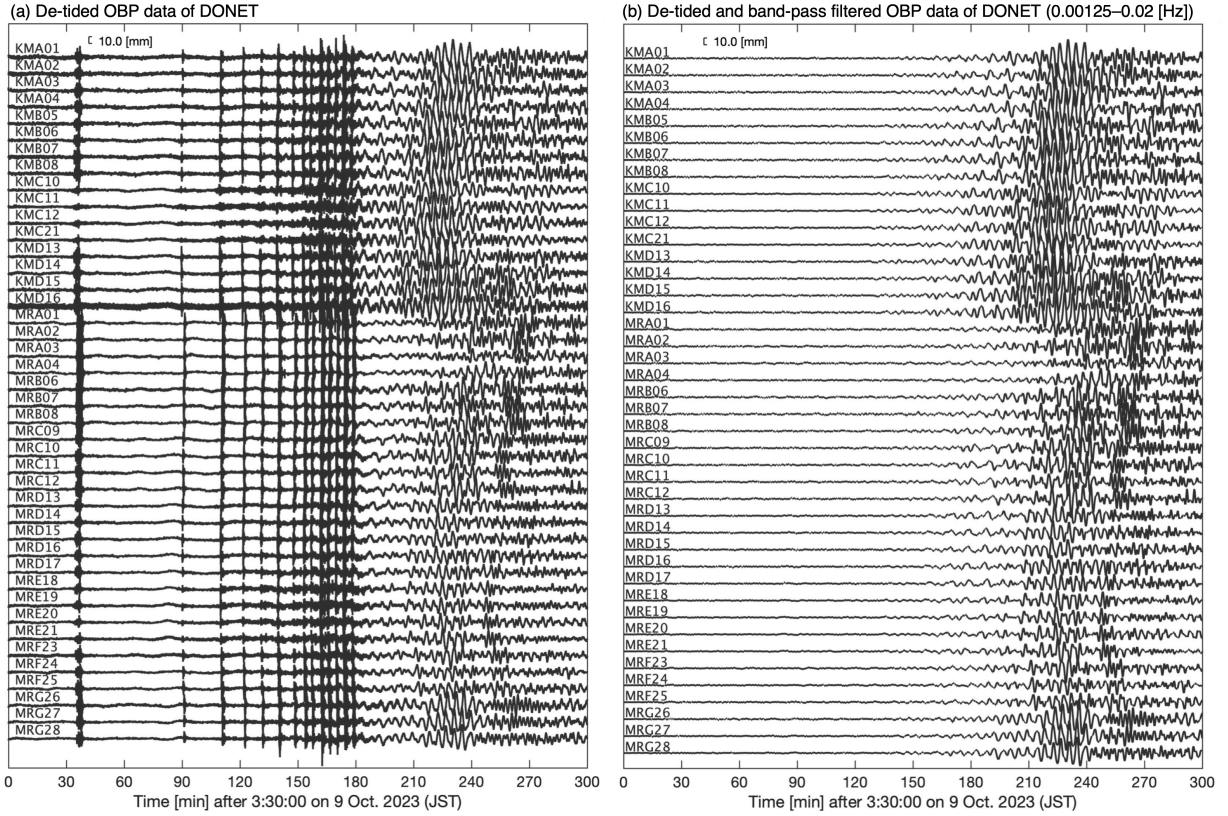


Figure 2. OBP data of DONET after 3:30:00 on 9 October 2023 (JST). **(a)** Data after removing the tidal trend by polynomial approximation, and **(b)** after the tidal-trend removal and the band-pass filter (0.00125–0.02 Hz), in the frequency range where tsunami signals are dominant. The amplitudes are in unit of water wave height [mm] converted from pressure, using $1.0 \text{ [Pa]} = 0.102 \text{ [mmH}_2\text{O]}$.

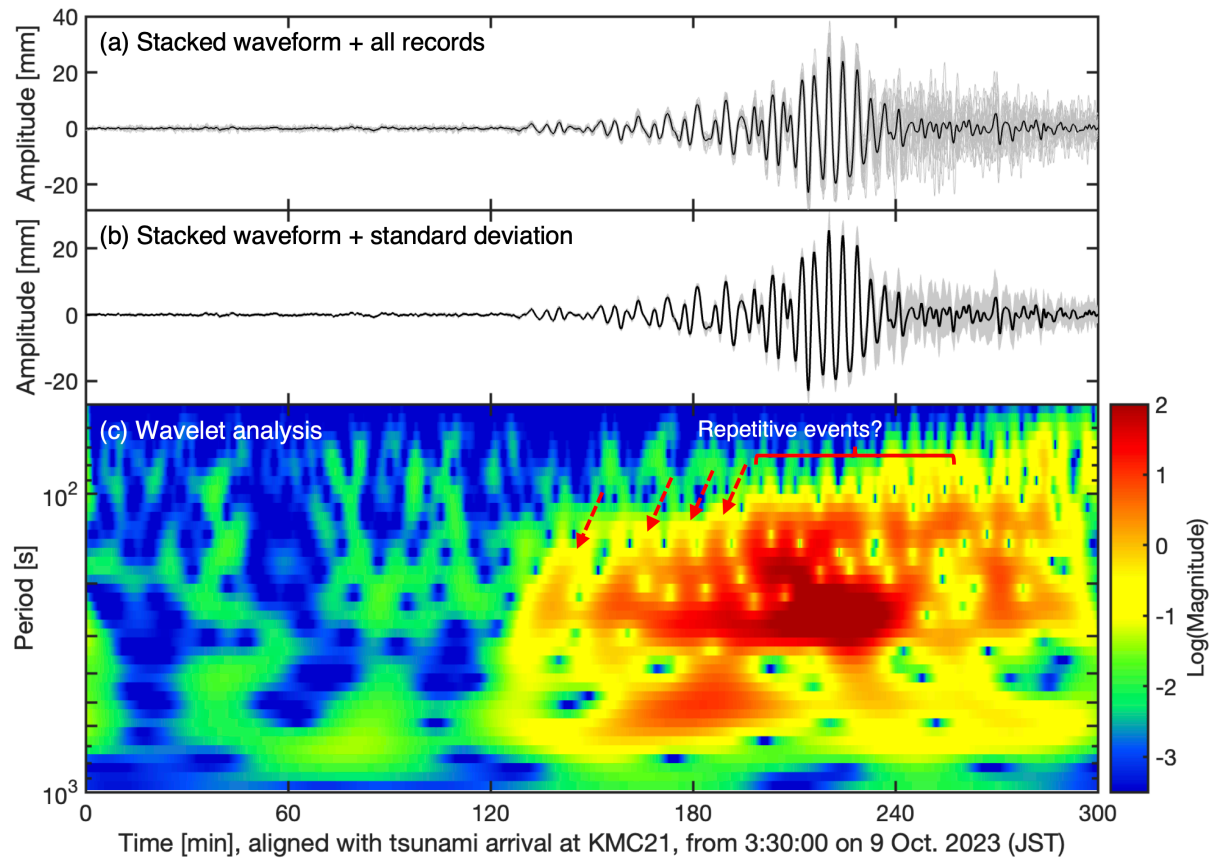


Figure 3. Waveform stacking of 16 OBP tsunami data from DONET1 (Table S2). (a) The stacked tsunami waveform (thick black line) and the 16 waveforms used for the stacking (thin gray lines). (b) The stacked waveform (thick black line) \pm the standard deviation (shaded by gray). (c) Wavelet analysis for the stacked waveform by the continuous wavelet transformation in MATLAB (Lilly, 2017). Red arrows and a curly bracket indicate multiple bands of amplitude peaks of tsunami wave trains.

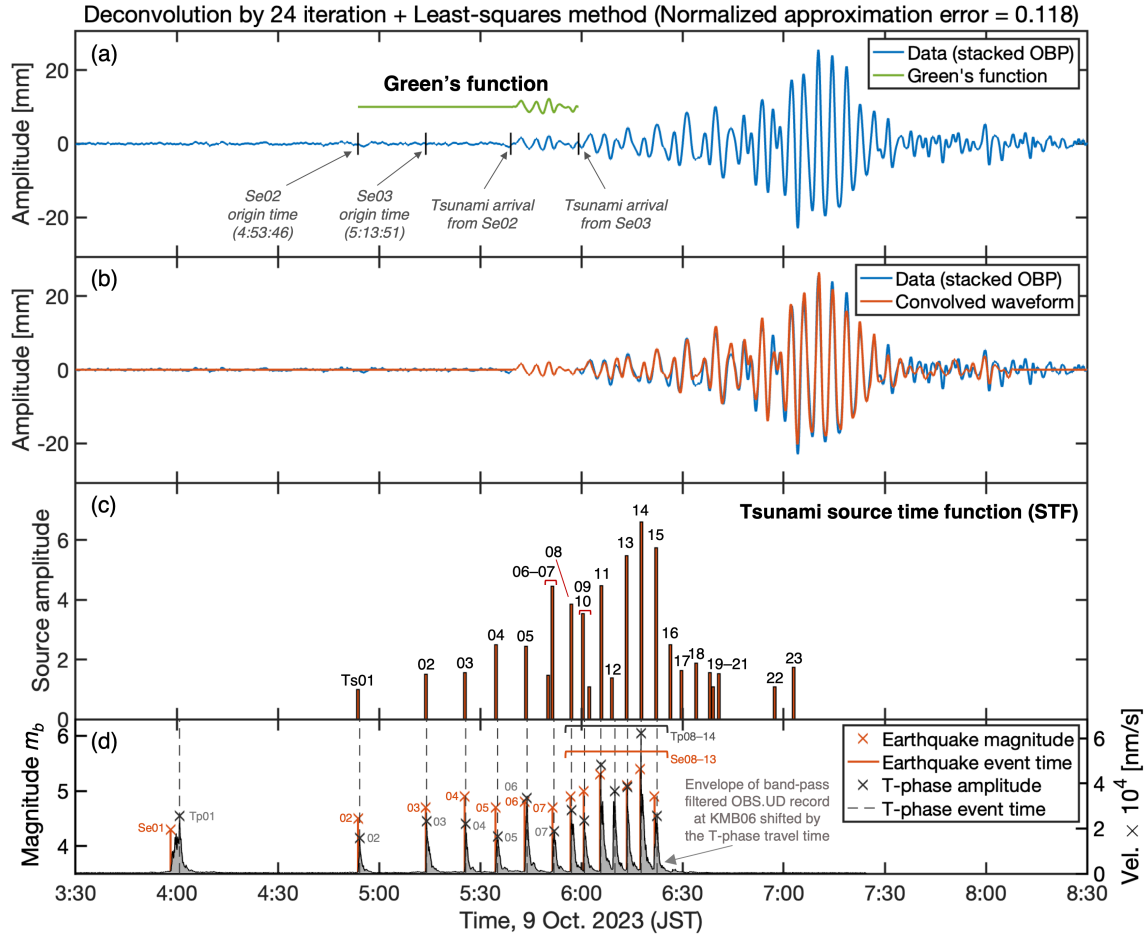


Figure 4. The tsunami STF by the iterative deconvolution (24 times) and the least-squares method. (a) The Green's function (green line) obtained from the stacked OBP tsunami waveform (blue line). (b) The convolved tsunami waveform (red line) compared with the stacked waveform. (c) Tsunami STF, composed of 23 source events (Ts01–Ts23; Table S3). The source amplitudes are relative to that of Ts01. (d) The temporal history of the seismic events (Se01–13) and the T-phase events (Tp01–14), and the envelope of the up-down component of OBS at KMB06, shifted backward in time by the T-phase travel time at 1.5 km/s (5.48 [min]) (gray shade).

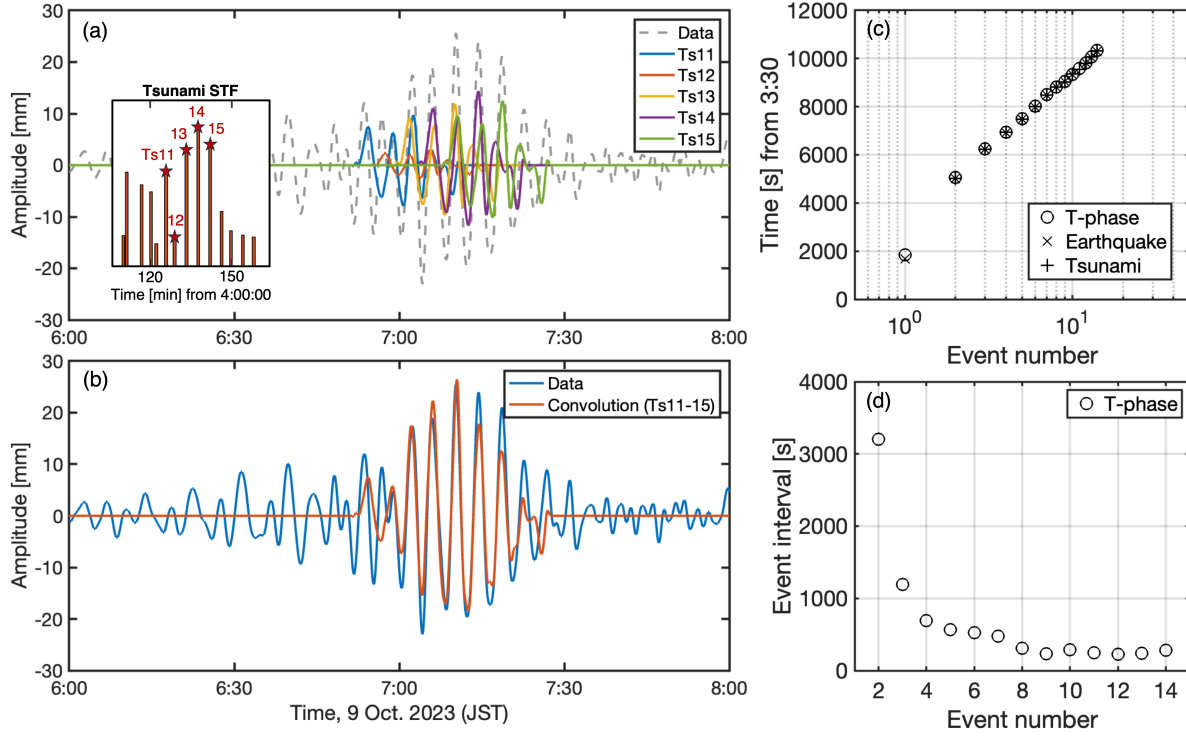


Figure 5. Tsunami waves of the later events. **(a)** The waveforms due to each event of Ts11–15, shown in the inset panel. **(b)** The convolved waveform with Ts11–15 (orange line) and the stacked waveform (blue line). **(c–d)** The relationship between **(c)** the event number and timing, for source events EV01–14, determined by tsunamis, seismic body-waves, and T-phases, and **(d)** between the event number and the interval times of the T-phase events.

References

- Abe, K. (1981). Physical size of tsunamigenic earthquakes of the northwestern Pacific. *Physics of the Earth and Planetary Interiors*, 27(3), 194–205. [https://doi.org/10.1016/0031-9201\(81\)90016-9](https://doi.org/10.1016/0031-9201(81)90016-9)
- Ewing, M., Tolstoy, I., & Frank Press. (1950). Proposed use of the T phase in tsunami warning systems. *Bulletin of the Seismological Society of America*, 40(1), 53–58. <https://doi.org/10.1785/BSSA0400010053>
- Fukao, Y., Sandanbata, O., Sugioka, H., Ito, A., Shiobara, H., Watada, S., & Satake, K. (2018). Mechanism of the 2015 volcanic tsunami earthquake near Torishima, Japan. *Science Advances*, 4(4), eaao0219. <https://doi.org/10.1126/sciadv.aao0219>
- Grilli, S. T., Tappin, D. R., Carey, S., Watt, S. F. L., Ward, S. N., Grilli, A. R., et al. (2019). Modelling of the tsunami from the December 22, 2018 lateral collapse of Anak Krakatau volcano in the Sunda Straits, Indonesia. *Scientific Reports*, 9(1), 11946. <https://doi.org/10.1038/s41598-019-48327-6>
- Hydrographic and Oceanographic Department, Japan Coast Guard. (2006). Database of the Maritime and Submarine Volcanoes in Japan. Retrieved October 14, 2023, from <https://www1.kaiho.mlit.go.jp/kaiikiDB/list-2.htm>
- Igarashi, G. (2000). A geodetic sign of the critical point of stress - strain state at a plate boundary. *Geophysical Research Letters*, 27(13), 1973–1976. <https://doi.org/10.1029/1999gl005443>
- Japan Meteorological Agency. (2023, October 9). Report on Earthquake near Torishima Island around 5:25 on October 9, 2023 (2nd report) (in Japanese). Retrieved October 19, 2023, from <https://www.jma.go.jp/jma/press/2310/09b/202310091100.html>
- Kanamori, H. (1972). Mechanism of tsunami earthquakes. *Physics of the Earth and Planetary Interiors*, 6(5), 346–359. [https://doi.org/10.1016/0031-9201\(72\)90058-1](https://doi.org/10.1016/0031-9201(72)90058-1)
- Kanamori, H., Ekström, G., Dziewonski, A., Barker, J. S., & Sipkin, S. A. (1993). Seismic radiation by magma injection: An anomalous seismic event near Tori Shima, Japan. *Journal of Geophysical Research*, 98(B4), 6511–6522. <https://doi.org/10.1029/92jb02867>

- 336 Kikuchi, B. Y. M., & Kanamori, H. (1982). Inversion of complex body waves. *Bulletin of the Seismological*
337 *Society of America*, 72(2), 491–506. x
- 338 Kodaira, S., Sato, T., Takahashi, N., Ito, A., Tamura, Y., Tatsumi, Y., & Kaneda, Y. (2007). Seismological
339 evidence for variable growth of crust along the Izu intraoceanic arc. *Journal of Geophysical Research*,
340 112(B5), B05104. <https://doi.org/10.1029/2006jb004593>
- 341 Kubota, T., Saito, T., & Nishida, K. (2022). Global fast-traveling tsunamis driven by atmospheric Lamb waves
342 on the 2022 Tonga eruption. *Science*, 377(6601), 91–94. <https://doi.org/10.1126/science.abo4364>
- 343 Lilly, J. M. (2017). Element analysis: a wavelet-based method for analysing time-localized events in noisy
344 time series. *Proceedings. Mathematical, Physical, and Engineering Sciences / the Royal Society*,
345 473(2200), 20160776. <https://doi.org/10.1098/rspa.2016.0776>
- 346 Maeno, F., Imamura, F., & Taniguchi, H. (2006). Numerical simulation of tsunamis generated by caldera
347 collapse during the 7.3 ka Kikai eruption, Kyushu, Japan. *Earth, Planets and Space*, 58(8), 1013–
348 1024. <https://doi.org/10.1186/BF03352606>
- 349 Matsumoto, H., Haralabus, G., Zampolli, M., & Özel, N. M. (2016). T - phase and tsunami pressure
350 waveforms recorded by near - source IMS water - column hydrophone triplets during the 2015 Chile
351 earthquake. *Geophysical Research Letters*, 43(24). <https://doi.org/10.1002/2016gl071425>
- 352 Michon, L., Villeneuve, N., Catry, T., & Merle, O. (2009). How summit calderas collapse on basaltic
353 volcanoes: New insights from the April 2007 caldera collapse of Piton de la Fournaise volcano.
354 *Journal of Volcanology and Geothermal Research*, 184(1), 138–151.
355 <https://doi.org/10.1016/j.jvolgeores.2008.11.003>
- 356 Mulia, I. E., Watada, S., Ho, T.-C., Satake, K., Wang, Y., & Aditiya, A. (2020). Simulation of the 2018
357 tsunami due to the flank failure of anak Krakatau volcano and implication for future observing
358 systems. *Geophysical Research Letters*, 47(14), e2020GL087334.
359 <https://doi.org/10.1029/2020gl087334>
- 360 National Research Institute for Earth Science and Disaster Resilience. (2019). NIED DONET [Data set].
361 National Research Institute for Earth Science and Disaster Resilience.
362 <https://doi.org/10.17598/NIED.0008>

- Okal, E. A. (2003). T Waves from the 1998 Papua New Guinea Earthquake and its Aftershocks: Timing the Tsunamigenic Slump. In J.-P. Bardet, F. Imamura, C. E. Synolakis, E. A. Okal, & H. L. Davies (Eds.), *Landslide Tsunamis: Recent Findings and Research Directions* (pp. 1843–1863). Basel: Birkhäuser Basel. https://doi.org/10.1007/978-3-0348-7995-8_4
- Okal, E. A. (2008). The generation of T waves by earthquakes. In R. Dmowska (Ed.), *Advances in Geophysics* (Vol. 49, pp. 1–65). Elsevier. [https://doi.org/10.1016/S0065-2687\(07\)49001-X](https://doi.org/10.1016/S0065-2687(07)49001-X)
- Paris, R. (2015). Source mechanisms of volcanic tsunamis. *Philosophical Transactions. Series A, Mathematical, Physical, and Engineering Sciences*, 373(2053). <https://doi.org/10.1098/rsta.2014.0380>
- Purkis, S. J., Ward, S. N., Fitzpatrick, N. M., Garvin, J. B., Slayback, D., Cronin, S. J., et al. (2023). The 2022 Hunga-Tonga megatsunami: Near-field simulation of a once-in-a-century event. *Science Advances*, 9(15), eadf5493. <https://doi.org/10.1126/sciadv.adf5493>
- Saito, T., & Furumura, T. (2009). Three-dimensional tsunami generation simulation due to sea-bottom deformation and its interpretation based on the linear theory. *Geophysical Journal International*, 178(2), 877–888. <https://doi.org/10.1111/j.1365-246X.2009.04206.x>
- Sandanbata, O., Watada, S., Satake, K., Kanamori, H., Rivera, L., & Zhan, Z. (2022). Sub - decadal volcanic tsunamis due to submarine trapdoor faulting at sumisu caldera in the Izu–Bonin arc. *Journal of Geophysical Research, [Solid Earth]*, 127(9), e2022JB024213. <https://doi.org/10.1029/2022jb024213>
- Sandanbata, O., Watada, S., Satake, K., Kanamori, H., & Rivera, L. (2023). Two volcanic tsunami events caused by trapdoor faulting at a submerged caldera near Curtis and Cheeseman islands in the kermadec arc. *Geophysical Research Letters*, 50(7), e2022GL101086. <https://doi.org/10.1029/2022gl101086>
- Satake, K., & Kanamori, H. (1991). Abnormal tsunamis caused by the June 13, 1984, Torishima, Japan, earthquake. *Journal of Geophysical Research*, 96(B12), 19933–19939. <https://doi.org/10.1029/91jb01903>
- Sugioka, H., Fukao, Y., Kanazawa, T., & Kanjo, K. (2000). Volcanic events associated with an enigmatic submarine earthquake. *Geophysical Journal International*, 142(2), 361–370. <https://doi.org/10.1046/j.1365-246x.2000.00153.x>

- Synolakis, C. E., Bardet, J.-P., Borrero, J. C., Davies, H. L., Okal, E. A., Silver, E. A., et al. (2002). The slump origin of the 1998 Papua New Guinea Tsunami. *Proceedings of the Royal Society of London. Series A: Mathematical, Physical and Engineering Sciences*, 458(2020), 763–789. <https://doi.org/10.1098/rspa.2001.0915>
- Tanioka, Y., & Satake, K. (1996). Fault parameters of the 1896 Sanriku Tsunami Earthquake estimated from Tsunami Numerical Modeling. *Geophysical Research Letters*, 23(13), 1549–1552. <https://doi.org/10.1029/96GL01479>
- Tappin, D. R., Matsumoto, T., Watts, P., Satake, K., McMurtry, G. M., Matsuyama, M., et al. (1999). Sediment slump likely caused 1998 Papua New Guinea tsunami. *Eos*, 80(30), 329. <https://doi.org/10.1029/99eo00241>
- Yamada, M., Mori, J., & Matsushi, Y. (2016). Possible stick - slip behavior before the Rausu landslide inferred from repeating seismic events. *Geophysical Research Letters*, 43(17), 9038–9044. <https://doi.org/10.1002/2016gl069288>
- Yamasato, H., Hamada, N., McCreery, C. S., Oliveira, F. J., Walker, D. A., & Talandier, J. (1993). T Waves Associated with Submarine Volcanic Eruptions in the Marianas Observed by Ocean Bottom Seismographs. *Journal of Physics of the Earth*, 41(2), 57–74. <https://doi.org/10.4294/jpe1952.41.57>